Thermal buckling of thin sheet related to cold rolling: Latent flatness defects modeling

Dinh Cuong Tran, Nicolas Tardif, Hamza El Khaloui, Ali Limam

Published in Thin-Walled Structures, Elsevier
http://dx.doi.org/10.1016/j.tws.2016.12.010

Thermal buckling of thin sheet related to cold rolling: latent flatness defects modeling

Dinh Cuong Tran[a], Nicolas Tardif[b], Hamza El Khaloui[b], Ali Limam[a]

*Corresponding author. e-mail: dinh-cuong.tran@insa-lyon.fr, nicolas.tardif@insa-lyon.fr, ali.limam@insa-lyon.fr

[a]Université de Lyon, INSA-Lyon, Laboratoire de Génie Civil et Ingénierie Environnementale, 20 Avenue Albert Einstein, Villeurbanne, France

[b]Université de Lyon, CNRS, INSA-Lyon, Laboratoire de Mécanique des Contacts et des Structures, UMR5259, F-69621 Villeurbanne, France

Abstract

In cold rolling of thin sheet metal, the interstand tension has a role to mitigate the wrinkling of the plate due to residual stress. When this mechanical loading is reduced up to full unloading, it can induce or increase elastic wave buckling, leading to latent flatness defects. An experimental work is proposed to study the relation between residual stresses, global tensile stresses and buckling for wavy edge flatness defects during the mechanical unloading. Residual stresses are generated by thermal loading. The wrinkling shape and thermal field are measured by optical full-field measurements. Finite Element simulation using a combination of a non-linear algorithm and a bifurcation analysis that take into account mid-surface imperfections can follow the wrinkling behavior.

Keywords

Thermal buckling, Rolling, Unloading, Latent flatness defect, Residual stress, Experiments, Modeling

1. Introduction

During cold rolling of thin sheets, wrinkling may occur due to compressive residual stresses (**Fig. 1**). These flatness defects can be classified into two categories: manifested and latent. Manifested means that the flatness defects occur during the rolling process when the interstand tension is prescribed, contrary to the latent flatness defects that may arise when this global tension is released. Manifested flatness defects have been discussed in several works using analytical and numerical approaches to study the buckling and post-buckling behavior of laminated strip [1, 2]. To the knowledge of the authors, the only experimental investigation is reported in our first paper [3]. The wrinkling behavior of thin sheets, due to self-equilibrating residual stresses and global tension that simulates the rolling stress state, is analyzed. It confirmed the major role of the tensile load on the critical load and the wrinkling modes but also the influence of initial mid-surface imperfections.

As for latent flatness defects, the problem is more complicated than that of the manifested flatness defects. To our knowledge, there are only few analyses in the literature. Most existing methods for measuring geometrical profiles and residual stress profiles are discussed in the works of D. Weisz-Patrault [4]. According to this author, the in-line shape measurement is essentially processed by optical methods. As for the residual stress profiles, two solutions are considered. Actual technologies use a detecting roll equipped with an array of sensors located close to the surface of the roll along its generatrix. They measure local deflection of the roll surface in order to deduce the residual stress distribution along the width of the sheet. The drawback of the method is its poor spatial resolution. D. Weisz-Patrault [4] developed a new formalism that enables to infer the residual stress profile by measuring the surface displacement of a hole under the surface of the detecting roll, knowing the free surface traction of the hole, by a semi-analytical Cauchy inverse method. The paper opens the way of technological design of new detecting roll.

Considering latent defects prediction, F.D. Fischer et al. [5] studied the buckling phenomena related to rolling and leveling of a thin plate with infinite length. By solving the eigenvalue problems using analytical solution and finite element analysis, the critical residual stresses distribution and the buckling characteristics are derived as a function of the global interstand tension. In [6], the buckling and post-buckling behavior of long strips and plates of finite length was investigated up to cut off and laid down on a rigid table. The linear and nonlinear analyses are performed using ABAQUS. For a given longitudinal residual membrane force

distribution, a strip subjected to a global tensile force buckles with a constant characteristic wavelength up to full unloading of the interstand tension. Moreover, the team showed the significant impact of the dead load on the wrinkle amplitude of the strip when sliding over or resting on a measuring table.

S. Abdelkhalek et al. [7] proposed a general rolling FEM model using coupled and non-coupled approaches to latent flatness predictions. Contrary to the above-mentioned works, the residual stress profile is calculated from the interaction between rolls and sheet. The uncouple approach neglects the bite/post-bite interaction. The stress field computed by the strip rolling model is directly transfered into a buckling model. In the coupled technique, the in-bite and out-of-bite stress pattern may be strongly coupled. The redistribution of the stress field caused by the buckling phenomenon is taken into account in the rolling model. The rolling model is Lam3/Tec3 which uses a steady state formulation based on streamline integration. Two buckling models are considered. The first model is inspired from study of Counhaye [8] and the second model is developed from the Asymptotic Numerical Method. The comparison of these models shows that a strong coupling is necessary to give a better solution of stress profiles and of wave shapes.

S. Abdelkhalek et al. [9, 10] also studied the behavior of the flatness defect during unloading using the Asymptotic Numerical Method. The modeling shows that during tension release, buckling begins in initial compression part and modifies the global internal stress distribution in the structure. This redistribution of stress field can transform a tensile zone into a compressive one where new defects may happen.

All above-mentioned studies are limited to analytical and numerical simulations. They are able to explain some manufacturing observations in a qualifying manner. No direct comparison to experimental results were performed. Moreover, the question of possible branching in the post-buckling response during unloading has not been fully addressed yet. Hence, the paper proposes experimental and numerical investigations of this phenomenon. The case of wavy edge flatness defect is analyzed.

The stress distribution in a strip during the rolling process is simulated by a thermo-mechanical loading. The interstand tension is simulated by a global mechanical tension. The self-equilibrating residual stresses, responsible for buckling, are modeled by local thermal patches. Thermal buckling and wrinkling of thin sheets have been studied for a long time. Reviews can be found in [11, 12]. Recently, Attipou et al. [13] considered the thermal

wrinkling behavior of thin membranes using a double scale Fourier series method. Jin et al. [14] quantified the buckling parameters of a laminated composite plate under a uniform temperature distribution using digital image correlation method. In our test, full-field measurements are performed to get the mid-surface imperfections, the wrinkling shape and the thermal field. This data allows analyzing in detail the experimental results and gives high-resolution inputs for numerical modeling.

The paper is divided in the following way. The experimental and numerical methods are presented first. Then, the results of a representative test and its numerical simulation are discussed. Finally, the conclusion is emphasized.

2. Experimental setup

The detailed description of the test procedure is presented in the previous paper [3]. The specimen (Fig. 2) is 800 mm long, 210 mm wide (Rolling direction - RD) and 0.332 mm thick. The raw material is a cold rolled and skin passed middle carbon steel whose elastic properties are: Young's modulus E = 205.7 GPa, Poisson's ratio $\nu = 0.28$, yield stress $\sigma_{0.2}$ = 420.8 MPa.

The experimental setup is showed in Fig. 3. The specimen is mounted to the frame using ball-jointed grips. The effective length of the plate (731 mm) is the inter-grips distance. During cold rolling, Rammerstorfer et al. [2] considers that the stress state of thin sheet between two rolling stands is stationary in the rolling direction. It is the combination of tensile stresses (interstand tension) and residual membrane stresses that is self-equilibrated in the transverse direction. A lever system is used to simulate the interstand tension. In addition to this stress, thermal stress induced by quartz infrared emitters simulates the self-equilibrating residual membrane stress distribution. The heating zone (width B0 = 25 mm, length L0 = 400 mm, red in Fig. 2) is located at the edges.

The temperature field is measured by an infrared camera whose accuracy is ± 2 °C. To set its emissivity parameter, thermocouples are spot-welded on the surface (TCi in Fig. 2). Moreover, the evolution of the 3D coordinates of the surface of the strip is measured by three-dimensional digital image correlation technique [15, 16] using VIC 3D commercial software [17]. Using this method, the typical theoretical error is ± 0.04 pixels [18]. With our experimental setup, the out-of-plane displacement resolution is about 0.01 mm ($1/30^{th}$ of the

thickness). A signal generator synchronizes all measurements with the acquisition frequency of 2.54 Hz.

The test procedure includes four steps. Firstly, the global tension is applied using the lever system. Then, a constant power is set to the generator of the quartz emitters. It induces a local heating of the strip until reaching a predefined temperature. Thereafter, the power generator is shut down and the temperature decreases progressively in free way. Finally, the lever system is unloaded in order to simulate the release of the interstand tension. In rolling, a quasi-static unloading is performed to ensure that no defects arise from dynamic effects. Here, the unloading rate is chosen so that it is slow enough to lessen the vibrations and the movement of stress waves that could influence the wrinkling modes. But it is also fast enough to ensure a small change in the temperature distribution and hence a small change in the simulated residual stress field that remains constant in the rolling process.

3. Numerical simulations

The commercial software Abaqus/Standard 6.13-4 [19] is used to simulate the experimental test. All model parameters (mesh, geometrical imperfection, material parameters and boundary conditions) are described in the previous paper [3]. Fig. 4 shows the numerical model. A coefficient of thermal expansion $\alpha = 1.2e^{-5}\ K^{-1}$ is chosen [20]. The plate remains in the elastic domain during the full loading-unloading procedure. The analysis comprises three steps: global tension loading, application of the evolving measured temperature field via the subroutine UTEMP and finally mechanical unloading.

A static calculation using the stabilization procedure is performed with the non-linear geometric mode in the first two steps. The stabilization procedure regularizes numerical instabilities induced by the meshed mid-surface imperfections. This method is validated in the previous paper [3]. In the last step, several methods are proposed to simulate the evolving wrinkling modes. It allows verifying the reliability of the numerical results and the capacity of each method. The choice of Abaqus solver algorithms [19] has been discussed in some works on linear buckling and post-buckling [21, 22]. In our case, Abaqus/Explicit is not applicable when temperature field is imported from Abaqus/Standard. In unstable analyses the instabilities are local (surface wrinkling or local buckling), global load control methods such as the Riks method are not appropriate. Moreover, the Riks method does not allow applying a change of temperature during the mechanical unloading step. The stabilization and Dynamic/Implicit method are compatible with the modeling of the wrinkling phenomenon in

quasi-static domain. These approaches allow following the evolution of wrinkling modes that change gradually. When a bifurcation occurs, the addition of a bifurcation step is necessary to capture the new equilibrium branch.

As was said previously, the loading part of the model was investigated in the previous paper [3]. Here, the analysis focuses on the mechanical unloading part of the test. The influence of the solver, the influence of the small variation of the measured thermal field during the unloading, and the influence of the boundary conditions (rotation around the horizontal axis Rx) are the main parameters of the study.

3.1. Stabilization method (S)

This approach can stabilize the unstable quasi-static problem by applying damping throughout the model. When local instability occurs, the deformation rate of that portion begins to increase, and locally released strain energy is dissipated due to the appended damping effect. The viscous forces introduced are sufficiently large to prevent instantaneous buckling but small enough not to affect the behavior significantly while the problem is stable. It means that to ensure the accurate solutions, the viscous forces are relatively small compared with the overall forces in the model. And the ratio of viscous damping to total strain energy does not exceed the dissipated energy fraction or any reasonable amount. Therefore, obtaining an optimal value for the damping factor is a manual process requiring trial and error until a converged solution is obtained and the dissipated stabilization energy is sufficiently small [19].

The viscous forces have the following form:

$$F_V = cM^*V \tag{1}$$

This force is added to the global equilibrium equations:

$$P - I - F_V = 0 \tag{2}$$

Where M* is an artificial mass matrix calculated with unity density, c is a damping factor, V is the vector of nodal velocities, P is the external load, and I is the internal force.

The equation solved in each Newton-Raphson iteration becomes:

$$\left(K_t + \frac{c}{\Delta t}M^*\right)du = R - cM^*\frac{\Delta u}{\Delta t} \tag{3}$$

Where K_t is the "static" tangent stiffness matrix, R is the force residual vector (P - I), du is the nodal displacement correction, Δt is the time increment, and Δu is the nodal displacement increment.

3.2. Dynamic/Implicit method: quasi-static (D)

The Dynamic/Implicit method in Abaqus/Standard uses implicit time integration to calculate the transient dynamic or quasi-static response of a system. It means that the operator matrix must be inverted and a set of simultaneous nonlinear dynamic equilibrium equations must be solved at each time increment. This solution is done iteratively using Newton's method. The quasi-static option is primarily interested in determining a final static response. These problems typically show monotonic behavior, and inertia effects are introduced primarily to regularize unstable behavior. To get a quasi-static solution, the backward Euler time integrator is used and very significant numerical damping is applied. This procedure is automatic in Abaqus software. The ratio of kinetic to internal energy is small to assure the accurate solution [19].

The equation of motion for dynamic problems can be represented as follows:

$$[M]\{\ddot{u}\} + [c]\{\dot{u}\} + [K]\{u\} = \{P\} \quad (4)$$

Where [M] is the mass matrix, $\{\ddot{u}\}$ is the acceleration vector, $\{\dot{u}\}$ is the velocities vector, {u} is the displacement vector, [c] is the damping matrix, [K] is the stiffness matrix, and {P} is the vector of applied loads.

The principle of backward Euler time integrator is showed by the following equations:

$$u_{t+\Delta t} = u_t + \Delta t \dot{u}_{t+\Delta t} \quad (5)$$

$$\dot{u}_{t+\Delta t} = \dot{u}_t + \Delta t \ddot{u}_{t+\Delta t} \quad (6)$$

$$-R_{t+\Delta t} = M\ddot{u}_{t+\Delta t} + (I - P)_{t+\Delta t} \quad (7)$$

Where R is the force residual vector.

4. Results

In this section, results and simulations of tests conducted with a mean global tensile stress $\bar{\sigma}$ = 50 MPa are presented. The reproducibility of the experimental results was checked.

The initial mid-surface imperfections of the specimen are measured by three-dimensional digital image correlation technique. The measured geometry is taken into account in the mesh. More details on the type of imperfections can be found in [3].

The loading procedure is showed in Fig. 5. When the relative temperature $\Delta\theta$ reaches the value of 60 °C at the position of TC2, the power generator of the infrared emitters is shut down. During the cooling, the mechanical unloading is performed gradually when $\Delta\theta$ = 34 °C. The unloading rate of tensile force is about 2.28 N/(mm.s). The thermal unloading rate is 0.69 °C/s at the location of TC2. The duration of the mechanical unloading is about 8.64 s.

During this unloading, the loss of temperature is about 6 °C. Fig. 6 shows the wrinkling profile for timestamps 1 to 4 depicted by a dot in Fig. 5. At the beginning of the mechanical unloading, mode 1 is the major mode (timestamp 1). When the tensile force decreases, the amplitude of existing wrinkles increases, and for certain critical tensile force distributions, new undulations appear from the geometrical imperfection (timestamp 2). When tensile force is close to zero, the wave mode switches to a global mode (timestamp 3). The global mode evolves until timestamp 4 and after timestamp 4, only the magnitude of the mode increases. Between both edges no phase relation is observed.

By taking the formalism of Fischer et al. [5] and our first paper [3], the membrane force per unit of width in sheet is the combination of a tensile force per unit of width Nt (calculated from the mechanical loading) and a self-equilibrating residual membrane force per unit of width Nr (thermal loading). Nr is determined from a static analysis on the free plate (without tensile membrane force and without initial geometric imperfections). It is subjected to the measured temperature. At the moment of mechanical unloading, the distribution of membrane force per unit of width at the center of the specimen is showed in Fig. 7. Nt varies in the transverse direction due to the mid-surface imperfections as discussed in [3]. Compared to the heating step [3], the residual stresses distribution (Nr) is less concentrated at the edges due to thermal diffusion.

The combined membrane force (sum of Nt and Nr) for timestamps 1 to 4 is plotted in Fig. 8. Just before the mechanical unloading (timestamps 1), a slight local compression appears in line 2 that is consistent with the small undulation seen in Fig. 6. During the unloading, the compression of the edges increases by essentially the global tension release (Nt). In the test, the compressive stresses are released by wrinkling of the edges.

Fig. 6(b) and (c) shows a good agreement between the calculation and the experimental test for timestamps 1 to 3. This means that both solvers are able to simulate the wrinkling process up to timestamp 3 as soon as the geometrical imperfections are taken into account in the mesh. In our case, the dynamic automatic regularization is sufficient to reproduce the wrinkling behavior whereas the choice of a good damping factor value in the static stabilization method is necessary. Likewise, the boundary condition of rotation around the X-axis has no influence on the solution because the wrinkling zone is far from the boundaries. In contrast, the variation of thermal field during the mechanical unloading has to be taken into account to best represent the experimental results. Nevertheless, the evolution of the thermal field negligibly affects the wavelength and the phase of the undulations. It is more influential on their amplitude.

From timestamp 3, both non-linear analyses are unable to follow the wrinkling branch of the experiment (timestamp 4) even if the evolution of the thermal field is taken into account. It calls for the occurrence of a bifurcation between timestamps 3 and 4.

To capture the post-buckling mode at timestamps 4, a bifurcation step is added at the end of the non-linear analysis at timestamp 3. In this step, the temperature is kept constant and a compressive force is applied. The normalized displacement of the first eigenmode of the bifurcation computation is compared to the normalized displacement between the two consecutive timestamps 3 and 4. The frequency of the cameras does not allow reducing this interval. Fig. 9 depicts the previously defined displacement profiles of line 1 and line 2. The bifurcation analysis seems to capture quite accurately the experimental observations.

The bifurcation force is showed in Table 1. It is compared to the experimental global force difference, which is measured between timestamps 3 and 4. Again, the most realistic eigenvalue corresponds to the model that takes into account the evolution of the thermal field during the unloading. Indeed, for this case, the stress state and the geometry of the specimen at timestamp 3, input of the bifurcation analysis, are closer to the experimental ones. The applied methods and the boundary condition affect very negligibly this result.

In addition to the dependence of the wrinkling on the residual stress distribution and amplitude, the latent wrinkling behavior depends on the initial mid-surface imperfections of the sheet. For our case, the plate has a complex shape (global and local defects). Just before the mechanical unloading (timestamp 1), the global mode dominates. However, small ripples are present. These undulations influence the evolving wrinkling modes when the tensile force

is reduced. In the study of Fischer et al. [5, 6], the perfect plate (without initial geometric imperfections) subjected to global tensile force and residual membrane force is considered. When the tensile force is monotonically decreased to a critical value, the strip buckles in the form of wrinkling whose characteristic length depends on the residual stress distribution and amplitude. This post-buckling shape does not evolve in terms of wavelength up to full unloading.

4. Conclusion

In the framework of cold rolling of thin strips, experiments are performed in order to simulate latent flatness defects. The residual stress responsible for wrinkling is modeled by thermal stresses. The experimental setup combines accurate full-field measurements of temperature and out-of-plane coordinates in order to give high-resolution input for model validation.

Contrary to other studies of the literature, the wrinkling mode evolves (wavelengths, phases) during the mechanical unloading. It is partly due to the geometrical configuration of the tests (small L0/B value in the present paper) but also due to the complex form of initial geometric imperfections present in the specimen. Moreover, at a certain value of tensile load, a bifurcation occurs. After the bifurcation, the global mode dominates and does not evolve (wavelengths, phase) up to full unloading.

Non-linear analyses with proper regularization methods can follow the wrinkling behavior during the mechanical unloading. It is efficient when the wrinkling mode changes progressively and the mid-surface imperfections are taken into account. But in some configurations, a bifurcation analysis is necessary to describe possible new equilibrium branches.

Acknowledgments

The study was performed in the framework of the ANR PLATFORM # 2012-RNMP-019-06. The authors would like to acknowledge all the participants of the project: ArcelorMittal, CEA, CEMEFMINES-PARISTECH, Constellium, Ecole Centrale of Paris, INSA Lyon and Paul Verlaine university of Metz.

References

[1] S. Abdelkhalek, P. Montmitonnet, N. Legrand, P. Buessler, Coupled approach for flatness prediction in cold rolling of thin strip, Int. J. Mech. Sci. 53 (2011) 661–675.

[2] F.G. Rammerstorfer, F.D. Fischer, N. Friedl, Buckling of free infinite strips under residual stresses and global tension, J. Appl. Mech. 68 (2000) 399–404.
[3] D.C. Tran, N. Tardif, A. Limam, Experimental and numerical modeling of flatness defects in strip cold rolling, Int. J. Solids Struct. 69–70 (2015) 343–349.
[4] D. Weisz-Patrault, Inverse Cauchy method with conformal mapping: Application to latent flatness defect detection during rolling process, Int. J. Solids Struct. 56–57 (2015) 175–193.
[5] F.D. Fischer, F.G. Rammerstorfer, N. Friedl, W. Wieser, Buckling phenomena related to rolling and levelling of sheet metal, Int. J. Mech. Sci. 42 (2000) 1887–1910.
[6] F.D. Fischer, N. Friedl, A. Noé, F.G. Rammerstorfer, A study on the buckling behaviour of strips and plates with residual stresses, Steel Res. Int. 76 (2005) 327–335.
[7] S. Abdelkhalek, H. Zahrouni, P. Montmitonnet, N. Legrand, M. Potier-Ferry, Latent and Manifested flatness predictions in thin strip cold rolling using a general rolling FEM model, Steel Res. Int. ICTP 2011 Special Issue-Bulk Metal Forming (2011) pages 111-116.
[8] C. Counhaye, Modélisation et contrôle industriel de la géométrie des aciers laminés à froid (modelling and industrial control of the geometry of cold rolled steels) (PhD dissertation), Université de Liège, Belgique, 2000.
[9] S. Abdelkhalek, H. Zahrouni, N. Legrand, M. Potier-Ferry, Post-buckling modeling for strips under tension and residual stresses using asymptotic numerical method, Int. J. Mech. Sci. 104 (2015) 126–137.
[10] S. Abdelkhalek, H. Zahrouni, N. Legrand, M. Potier-Ferry, A study of flatness defect in strip rolling occurred in tension unloading, in: AIP Conf. Proc., AIP Publishing, 2016: pp. 1–4.
[11] T.R. Tauchert, Thermally Induced Flexure, Buckling, and Vibration of Plates, Appl. Mech. Rev. 44 (1991) 347–360.
[12] E.A. Thornton, Thermal Buckling of Plates and Shells, Appl. Mech. Rev. 46 (1993) 485–506.
[13] K. Attipou, H. Hu, F. Mohri, M. Potier-Ferry, S. Belouettar, Thermal wrinkling of thin membranes using a Fourier-related double scale approach, Thin-Walled Struct. 94 (2015) 532–544.
[14] T. Jin, N.S. Ha, V.T. Le, N.S. Goo, H.C. Jeon, Thermal buckling measurement of a laminated composite plate under a uniform temperature distribution using the digital image correlation method, Compos. Struct. 123 (2015) 420–429.
[15] T.C. Chu, W.F. Ranson, M.A. Sutton, Applications of digital-image-correlation techniques to experimental mechanics, Exp. Mech. 25 (1985) 232–244.
[16] P.F. Luo, Y.J. Chao, M.A. Sutton, W.H. Peters, Accurate measurement of three-dimensional deformations in deformable and rigid bodies using computer vision, Exp. Mech. 33 (1993) 123–132.
[17] Vic-3D, Correlated Solutions Inc., Vic-3D User Manual. Columbia, USA, (2010). http://correlatedsolutions.com/vic-3d/.
[18] T.L. Jin, N.S. Ha, N.S. Goo, A study of the thermal buckling behavior of a circular aluminum plate using the digital image correlation technique and finite element analysis, Thin-Walled Struct. 77 (2014) 187–197.
[19] ABAQUS, ABAQUS Theory Manual and Analysis User's Manual (Version 6.12). Dassault Systèmes Simulia Corp. Providence, RI, USA, (2014). http://www.3ds.com/products-services/simulia/products/abaqus/.

[20] M. De Strycker, L. Schueremans, W. Van Paepegem, D. Debruyne, Measuring the thermal expansion coefficient of tubular steel specimens with digital image correlation techniques, Opt. Lasers Eng. 48 (2010) 978–986.
[21] L. Lanzi, A numerical and experimental investigation on composite stiffened panels into post-buckling, Thin-Walled Struct. 42 (2004) 1645–1664.
[22] T. Kobayashi, Y. Mihara, F. Fujii, Path-tracing analysis for post-buckling process of elastic cylindrical shells under axial compression, Thin-Walled Struct. 61 (2012) 180–187.

Figure captions

Fig. 1. Flatness defects in rolling [1].

Fig. 2. Specimen, viewed from the infrared camera (IR).

Fig. 3. Experimental setup.

Fig. 4. Numerical model.

Fig. 5. Relative temperature (thermocouple TC2) and tensile membrane force per unit of width as a function of time.

Fig. 6. (a) Out-of-plane displacement fields. (b) Out-of-plane displacement profiles over line 1. (c) Out-of-plane displacement profiles over line 2. Timestamps from 1 to 4.

Fig. 7. Membrane force per unit of width in the transverse direction at the center of the specimen corresponding to timestamps 1.

Fig. 8. Sum of Nt and Nr for timestamps 1-4 at the center of the specimen. Nt varies with mechanical unloading. Nr varies with the less pronounced thermal evolution.

Fig. 9. W-normalized between test and bifurcation analysis. (a) Line 1. (b) Line 2.

Table captions

Table 1

Comparison of bifurcation force ΔNt (N/mm).

Test	S, Rx free, Δθ fix	S, Rx free, Δθ vary	S, Rx fix, Δθ vary	D, Rx free, Δθ vary
1.106	1.242	1.049	1.047	1.051

Figure1

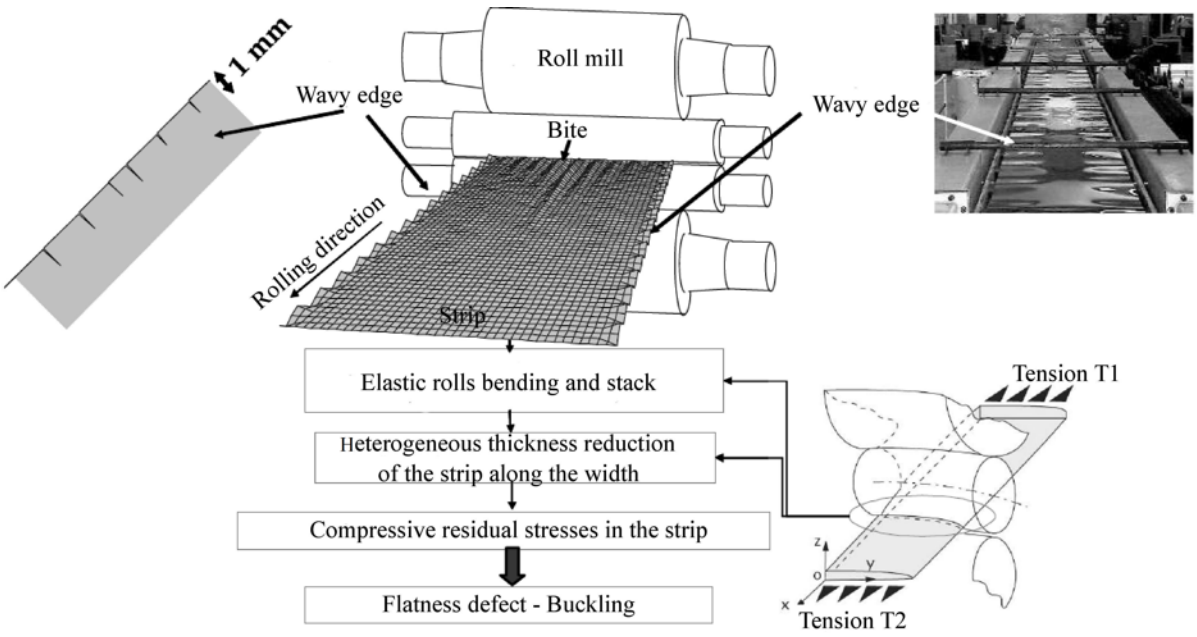
1 mm
Wavy edge
Roll mill
Bite
Wavy edge
Rolling direction
Strip
Elastic rolls bending and stack
Heterogeneous thickness reduction of the strip along the width
Compressive residual stresses in the strip
Flatness defect - Buckling
Tension T1
Tension T2

Figure 2

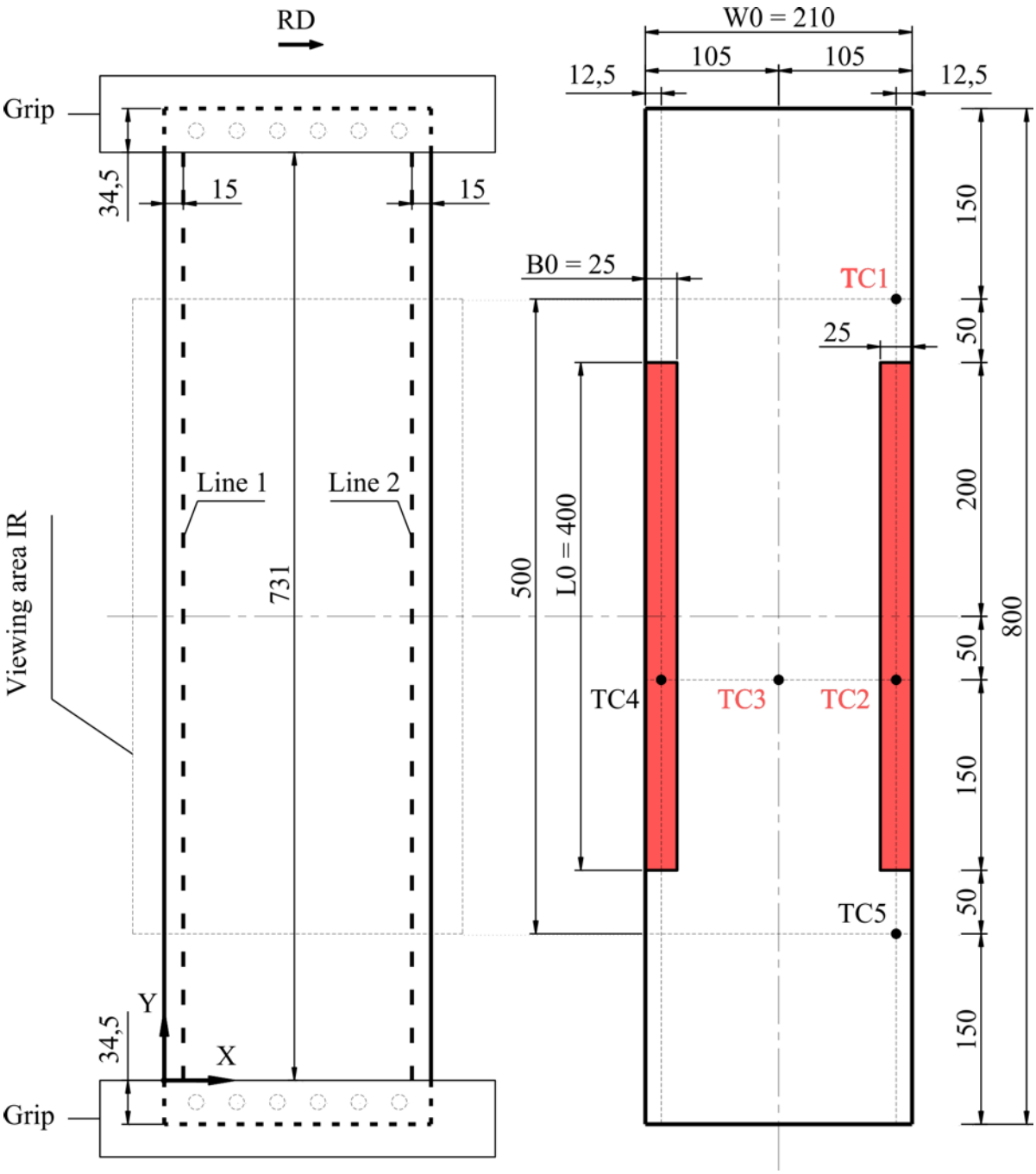
RD
Grip
34,5
15
15
Line 1
Line 2
731
Viewing area IR
Y
X
34,5
Grip
W0 = 210
105
105
12,5
12,5
B0 = 25
TC1
25
150
50
200
50
150
50
150
800
500
L0 = 400
TC4
TC3
TC2
TC5

Figure 3

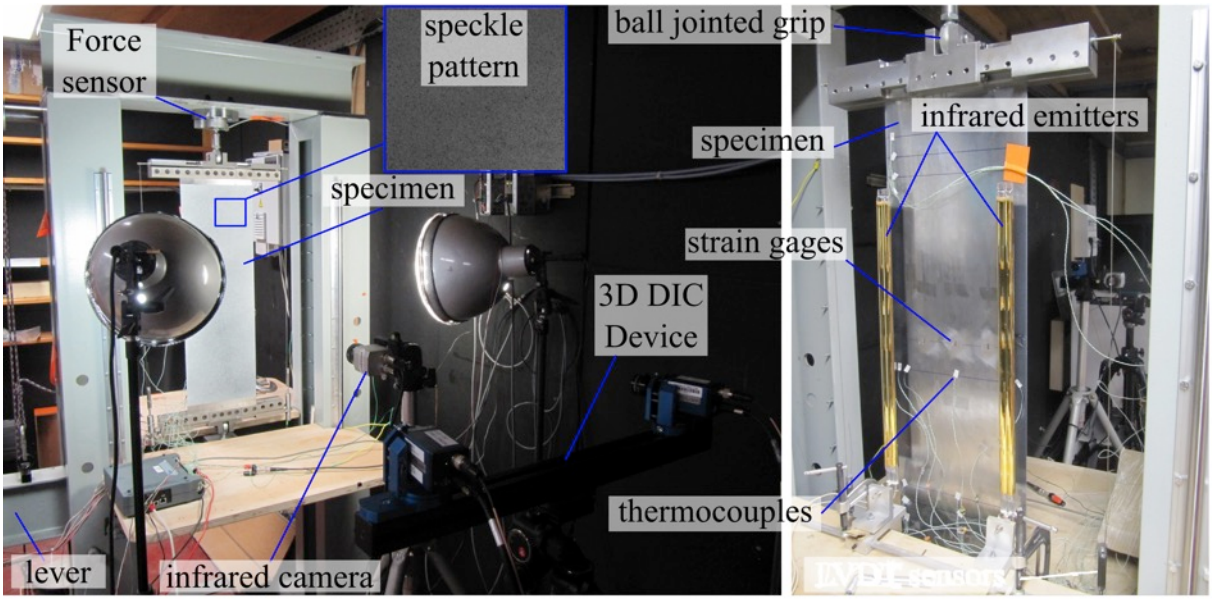

(a) Full field measurements face (b) Heated face

Figure 4

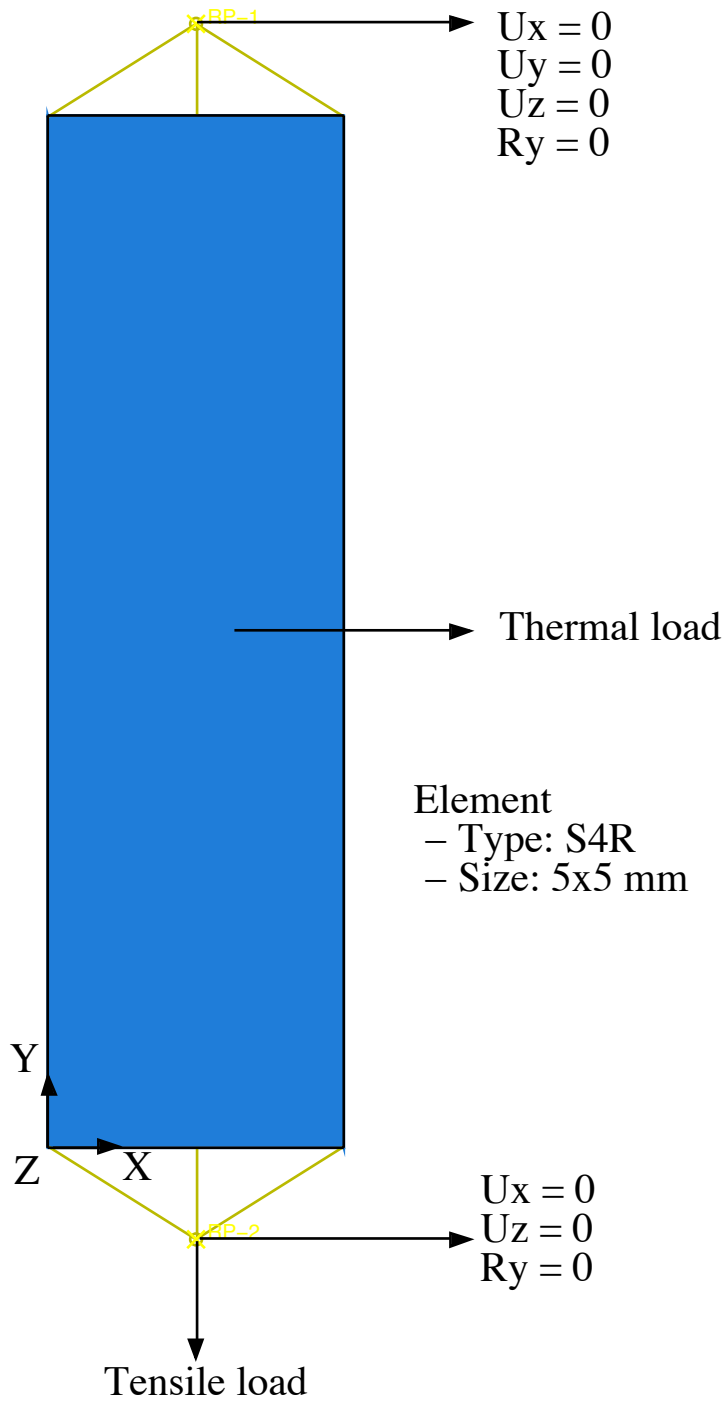
RP-1
Ux = 0
Uy = 0
Uz = 0
Ry = 0
Thermal load
Element
– Type: S4R
– Size: 5x5 mm
Y
Z
X
RP-2
Ux = 0
Uz = 0
Ry = 0
Tensile load

Figure 5

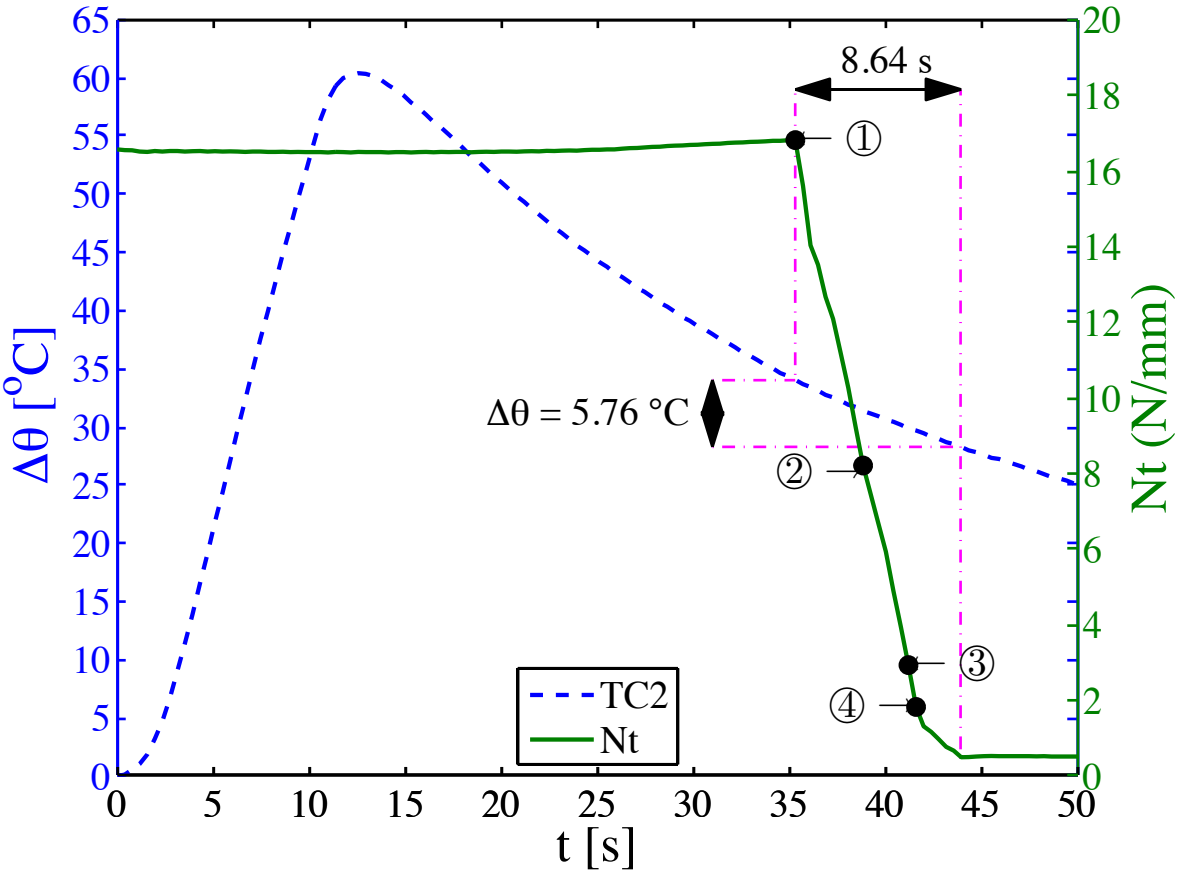
8.64 s
①
②
③
④
Δθ = 5.76 °C
TC2
Nt
Δθ [°C]
Nt (N/mm)
t [s]
0
5
10
15
20
25
30
35
40
45
50
55
60
65
2
4
6
8
12
14
16
18

Figure 6

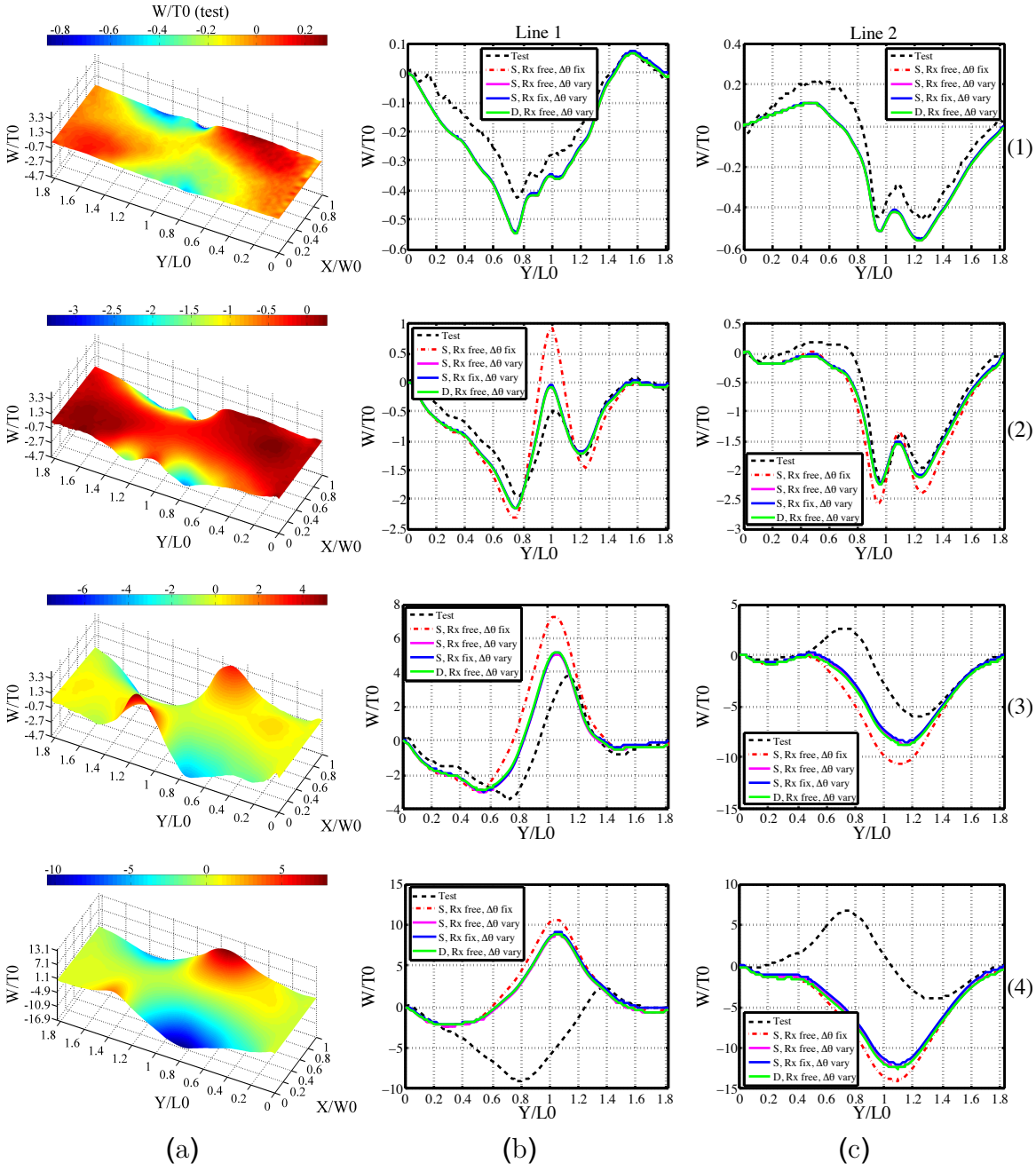
W/T0 (test)
Line 1
Line 2
Test
S, Rx free, Δθ fix
S, Rx free, Δθ vary
S, Rx fix, Δθ vary
D, Rx free, Δθ vary
W/T0
Y/L0
X/W0
(1)
(2)
(3)
(4)
(a)
(b)
(c)

Figure 7

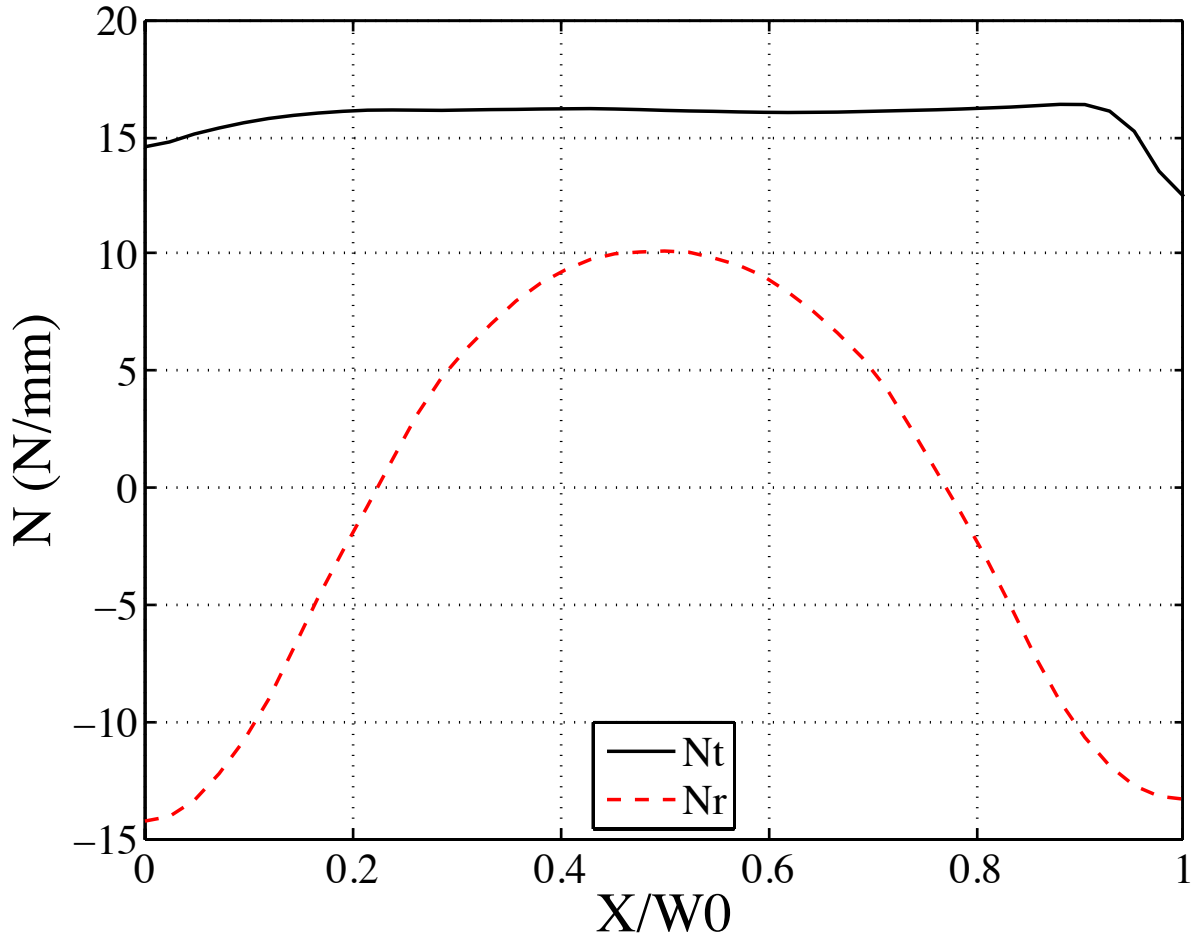

Figure 8

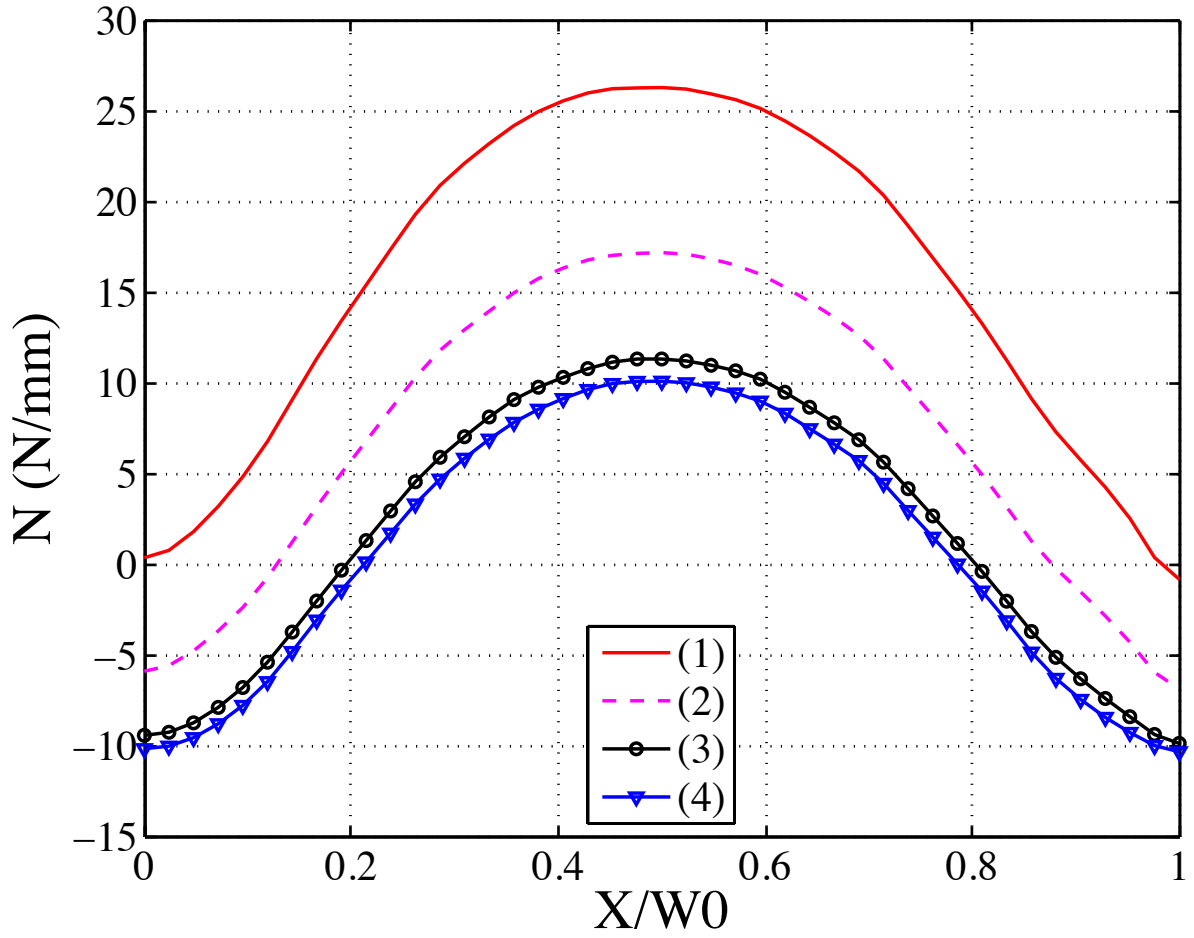

Figure 9

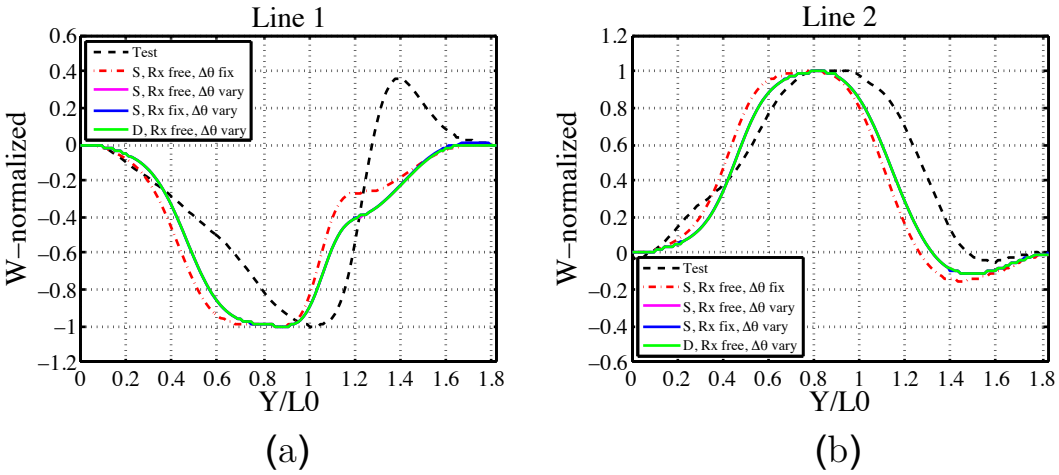
Line 1
W−normalized
Y/L0
Test
S, Rx free, Δθ fix
S, Rx free, Δθ vary
S, Rx fix, Δθ vary
D, Rx free, Δθ vary
Line 2
W−normalized
Y/L0
Test
S, Rx free, Δθ fix
S, Rx free, Δθ vary
S, Rx fix, Δθ vary
D, Rx free, Δθ vary

(a) (b)